APPENDICES

APPENDIX A

Photomicrographs

Key to abbreviations used in descriptions of photomicrographs:

BSE	back scattered electron mode—microprobe
SEM	scanning electron microscope
PPL	plane polarized light—optical microscope
XPL	cross polarized light—optical microscope
WRL	white reflected light—optical microscope
BRL	blue reflected light—fluorescence microscope
O-F	opaque-fluorescent cement (PPL & BRL)
P-F	pale-fluorescent cement (PPL & BRL)

Photo 1. Saprolite (#90-06B), Coyote Rd, Nevada City (PPL). View shows the granitic saprolite fabric comprised of quartz (white), kaolinized mica books (KM), zircon (Z), domains of coarse-grained kaolinite with vermicular morphologies (a), domains of fine-grained massive kaolinite (b), and a network of packing voids (c). O-F cement (black) saturates kaolinized mica and O-F particulate morphologies are associated with the coarser grained kaolinite (a) and at lower left of photo.

Photo 2. Saprolite (#90-07), Coyote Rd, Nevada City (BSE). View shows myrmekitic quartz fabric (a) at a boundary between a zone of fine-grained kaolinite (black) and coarse-grained kaolinite (gray). Remnant sericite flakes at "b"(white) occur among kaolinite stacks and vermicular morphologies.

Photo 3. Saprolite (#90-06B), Coyote Rd, Nevada City (SEM). View shows the typical microfabric in domains of fine-grained massive kaolinite composed of randomly arranged discrete particles and slightly larger stacks of kaolinite.

Photo 4. Saprolite (#90-06B), Coyote Rd, Nevada City (SEM). View shows the microfabric typical of coarse-grained kaolinite domains composed of large vermicular morphologies and stacks with a finer grained kaolinite matrix.

Photo 5. Saprolite (#90-07), Coyote Rd, Nevada City (BSE). View shows vermicular kaolinite (gray) with imbedded remnant layers of sericite (white).

Photo 6. Saprolite (#90-10), Coyote Rd, Nevada City (SEM). View shows randomly oriented flakes of sericite in a partially altered granitic xenolith. Note the resemblance of the irregular shapes and re-entrant grain margins of sericite platelets (a) to similar margin shapes and dimensions of individual kaolinite platelets in the vermicular forms exhibited in Photo 4.

Photo 7. Saprolite (#90-06B), Coyote Rd, Nevada City (SEM). View shows a kaolinized mica book (KM) embedded in the kaolinite matrix (K).

Photo 8. Saprolite (#90-07), Coyote Rd, Nevada City (BSE). View shows remnant biotite layers (bright) in a kaolinized mica book.

Photo 9. Saprolite (#90-07), Coyote Rd, Nevada City (BSE). View shows aggregate microfabric typical of much of the kaolinite fabric in the saprolite. The aggregate microfabric is characterized by relatively large kaolinite particles (white) enveloped by a matrix of smaller particles (a). This particular zone of fabric is also saturated with O-F cement (PPL). The O-F cement is the optical petrographic manifestation of amorphous silica cement (organo-siliceous) which saturates the kaolinite fabric and appears dark gray (b). The amorphous silica cement commonly forms meniscus shaped drapes between kaolinite particles and entrains spherical microvoids.

Photo 10. Saprolite (#90-07), Coyote Rd, Nevada City (BSE). View shows "spongy" microfabric in zones with high concentrations of O-F cement. The spongy microfabric is comprised of a multitude of spherical microvoids entrained in the cement with diameters of <1 μm. Image brightness and contrast was altered to optimize appearance of the amorphous cement. Kaolinite particles appear white.

Photo 11. Saprolite (#90-06B), Coyote Rd, Nevada City (PPL). View shows saprolite fabric comprised of quartz (white) arranged in its original position in the granitic fabric; kaolinized mica (KM) with original book structures disrupted and saturated with O-F cement; and sand-sized clay aggregates (micropeds) composed of fine-grained kaolinite (a) segregated by a network of packing voids. Homogenized "dirty" kaolinite fabric is produced by burrowing organisms (b). O-F cement concentrations occur in the center of some micropeds (c). The O-F cement occurring in the microped at "d" is a spherical enclosure that inhibited blue epoxy from impregnating the clay fabric on its interior. The orange-brown color is the true color of the clay (this thin section was not stained for feldspar).

Photo 12. Saprolite (#90-07), Coyote Rd, Nevada City (BRL). View shows zone of kaolinite fabric saturated by P-F cement (yellow). Kaolinite fabric surrounding cemented zone is impregnated with non-fluorescent blue epoxy (blue-gray). Adjacent quartz grains appear black. P-F cement also fills fractures in quartz grains in the saprolite fabric and appears yellowish orange in the photo.

Photo 13. Oxic horizon (#91-29), library site, Nevada City (PPL). View shows sand-sized kaolinite aggregates (micropeds) segregated by a network of packing voids. Micropeds are enveloped by P-F cement coatings which occur symmetrically and equidistant from packing voids (a). O-F cement coatings envelop some of the micropeds (b) and O-F cement concentrations occur at the center of others (c). The clay at the interior of micropeds enveloped by O-F cement was sealed from epoxy impregnation. Red plagioclase stain saturated the interior clay fabric after the thin section was cut (d).

Photo 14. Oxic horizon (#91-29), library site, Nevada City (BRL). View shows microped at "c" in Photo 13. P-F cement coating appears yellow (a) and O-F cement concentration in the center of the microped appears orange-yellow (b). Non-fluorescent blue epoxy fills packing voids and porous areas of kaolinite fabric (dark blue). A third fluorescent cement (bright white) occurs adjacent to packing voids.

Photo 15. Oxic horizon (#91-29C), library site, Nevada City (PPL with WRL). View shows arrangement of incipient iron oxide precipitation at margins of iron oxide segregations (mottles). Hematite (red) is concentrated along sites of O-F cement coatings (a). Goethite (G) appears yellow and occurs predominantly within the area of diffuse O-F cement (b) which has a pale yellow/cream color in white reflected light.

Photo 16. Upper pallid horizon (#91-28), library site, Nevada City (PPL). View shows kaolinized mica books in a thoroughly bioturbated kaolinite matrix (blue-gray). O-F cement coatings appear black. Blue epoxy fills packing voids. The clay fabric on the interior of O-F cement enclosures appear brown because they were sealed off from blue epoxy impregnation. O-F cement coatings traversing the clay fabric also pass through kaolinized mica grains (a).

Photo 17. Upper pallid horizon (#91-28), library site, Nevada City (SEM). View shows homogenized kaolinite microfabric in zone of bioturbation.

Photo 18. Ione mudstone (#89-06), Bacon Pit (SEM). View shows arrangement of clay particles in mudstone fabric. Individual kaolinite platelets of <1 μm in size are oriented in a parallel face-to-face arrangement within floccules (a). Adjacent floccules are arranged both face-to-face and edge-to-face (b).

Photo 19. Ione sandstone (#90-23), library site, Nevada City (PPL). View shows quartz (white) and feldspar grains (F) enveloped by detrital mud matrix. The homogeneous clay matrix appears milky blue (a). Packing voids are developed in the clay matrix (b). O-F cement coatings occur in the clay matrix symmetrically on both sides of packing voids. Red plagioclase stain saturated the clay in the interior of the enclosures formed by O-F cement coatings after the thin section was cut. Sand-sized detrital clay aggregates are common (c). Grain shaped voids in the mud matrix were left by the selective dissolution of the most weatherable minerals (d). Some feldspar grains show the effects of dissolution along perthitic lamellae (e).

Photo 20. Ione sandstone (#92-30), library site, Nevada City (PPL with WRL). View shows angular quartz grains in an open packing fabric produced by the dissolution of weatherable minerals and clay aggregates. Pore-lining illuvial clay coatings occur in most of the pores and exhibit a pale yellow color (a). Iron oxide staining in outcrop is produced by iron oxide precipitation (red) which only occurs associated with the illuvial clay coatings (b).

Photo 21. Intervolcanic sandstone (#91-08), Baxter (PPL). View shows sandstone composed of fine- to medium-grained quartz, plagioclase, biotite, volcanic rock fragments, and glass shards occurring with coarse-grained detrital pedogenic clay aggregates. A pedogenic clay aggregate derived from the underlying tuff is enveloped by a P-F coating (a). Its identity is unequivocal because of the abundant sponge spicules occurring within it. A plastic subspherical kaolinite aggregate containing vermicular morphologies was deformed by compression and squeezed into a narrowing opening between hard framework grains (b). The deformed kaolinite aggregate conforms to the grain shape of the impinging hard framework grain (c). The consistently larger grain size of lower density clay aggregates indicates that they were hydrodynamically equivalent to the smaller and denser quartz and feldspar grains. The opaque particles of high relief occurring in the kaolinite aggregate (upper left) and the volcanic clay aggregate (right) are voids trapped in the interstices in the clay fabrics.

Photo 22. Ione sandstone (#91-27B), Quaker Hill (PPL). View shows sandstone fabric comprised of quartz (white), K-feldspar (K), plagioclase (P), and detrital pedogenic kaolinite aggregates. Adjacent clay aggregates possess varying microfabrics with some possessing O-F cement concentrated at their centers (a). Compare with similar features occurring in the Oxisol at "c" in Photo 11. O-F particulate morphologies occur in coarser grained aggregates (upper left of photo). Most clay aggregates formed pseudomatrix when they were deformed by impinging rigid framework grains (b). The plastic nature of the clay aggregates is demonstrated by the manner in which the clay fabric was squeezed into narrow openings between rigid grains (c). The boundaries between adjacent clay aggregates in contact are delineated by abrupt changes in clay microfabric (d). Remnants of incompletely altered precursor grains sometimes occur imbedded in the matrix of clay aggregates (e).

Photo 23. Sandstone, Pattani Basin, Gulf of Thailand (BSE). View shows typical occurrence of authigenic kaolinite (K) filling secondary dissolution pores after feldspar. The authigenic pore-filling kaolinite is characterized by relatively homogeneous microfabric varying only slightly from pore to pore. Quartz grains and quartz overgrowths appear white.

Photo 24. Ione sandstone (#91-17), Old Sand Plant, Ione (BSE). View shows typical fabric of well sorted Lower Ione sandstones. Three detrital kaolinite aggregates with dramatically different microfabrics were deformed by impinging quartz grains (gray) and formed pseudomatrix. Heavy minerals (white) occur in a slightly smaller modal grain size than quartz and are commonly concentrated along laminae. The boundaries of adjacent clay aggregates are distinguished by an abrupt change in microfabric (a). The boundaries of clay aggregates with primary pores are commonly marked by a meniscus which drapes between quartz grains (b). The image shows the grain size difference between quartz and hydrodynamically equivalent detrital clay aggregates of lower density. The squashed clay aggregates form "gaps" in the sandstone fabric.

Photo 25. Sandstone, Pattani Basin, Gulf of Thailand (BSE). View shows the relatively homogeneous micromorphology and particle size distribution of pore-filling diagenetic kaolinite. In plan view, diagenetic kaolinite commonly forms euhedral hexagonal platelets (a). The uniform particle size distribution of diagenetic kaolinite results in relatively greater microporosity and better permeability than the pedogenic aggregate microfabric (Photo 26).

Photo 26. Ione sandstone (#89-09), Apricum Hill (BSE). View shows the pedogenic aggregate microfabric typical of many sand-sized kaolinite aggregate clasts in Ione sandstones. The aggregate microfabric is comprised of coarse- and fine-grained kaolinite particles (light gray) with amorphous siliceous-rich cement (dark gray). The amorphous cement forms meniscus shaped drapes between the kaolinite particles and commonly entrains spherical microvoids (a) which appear as diffuse O-F cement or discrete opaque particles in the clay fabric (PPL). Compare this pedogenic microfabric with the diagenetic pore-filling microfabric in Photo 25.

Photo 27. Ione sandstone (#91-17), Old Sand Plant, Ione (PPL). View shows well-sorted, bimodal, fine- to medium-grained kaolinitic sandstone. Hydrodynamically equivalent quartz and detrital clay clasts comprise the sandstone fabric. K-feldspar (K) and heavy minerals including amphibole (A) occur in trace amounts. Little post-depositional compaction has occurred and quartz cement is absent. The clay aggregates are concentrated in a larger modal grain size compared to quartz because of their inherent microporosity and lower bulk density. The occurrence of larger clay aggregates results in "gaps" in the sandstone fabric. The clay aggregates form pseudomatrix as result of deformation between rigid framework grains. Adjacent clay aggregates exhibit drastic variations in microfabrics ranging from fine-grained massive kaolinite (a) to coarse-grained kaolinite with vermicular morphologies (b). Clay aggregates commonly possess remnant O-F cement coatings (c). Amphibole grains show no signs of post-depositional weathering.

Photo 28. Ione sandstone (#89-29), Jones Butte (PPL). View shows muddy sandstone fabric comprised of fine-grained, angular quartz with trace amounts of K-feldspar (K) in a matrix-supported relationship with disaggregated detrital mud ("dirty" blue green). Medium-grained detrital kaolinite aggregates are distinguishable from disaggregated mud by their homogeneous milky blue color and sub-spherical shapes (a). Some clay aggregates contain O-F cement particulate morphologies (center of photo). O-F cement coatings form 1–3 mm long enclosures across the clayey sandstone fabric (b) indicative of *in situ* development. Red plagioclase stain invaded the unimpregnated clay fabric on the interior of the O-F coatings after the thin section was cut.

Photo 29. Ione sandstone (#89-09), Apricum Hill, Ione (PPL). View shows a well sorted, medium-grained Ione sandstone with detrital clasts comprised of quartz (white), kaolinized mica books (KM), K-feldspar (K), zircon (Z), and abundant sand-sized kaolinite aggregates deformed between rigid grains forming pseudomatrix. Adjacent clay aggregate boundaries are delineated by variations in their microfabric and amounts of O-F cement (a), or remnants of O-F cement coatings (b). Compression produced by impinging rigid grains caused swirls or concentric drape lines of O-F cement in the fabric of the adjacent clay aggregate (c). Incompletely altered remnants of the precursor mineral (probably feldspar) are visible in some clay aggregates (d).

Photo 30. Ione sandstone (#89-09), Apricum Hill, Ione (XPL). Cross-polarized view of Photo 29. Adjacent clay aggregates exhibit variable birefringence because of their differing microfabrics and crystallite sizes. Compression of the clay aggregate fabric adjacent to impinging rigid grains commonly causes platy or micaceous clay particles to realign parallel to the rigid grain margins. This phenomenon is often manifested as slightly higher birefringence of the clay fabric (a). Such higher birefringence of the clay fabric along rigid grain margins could be mistaken for authigenic illite. Quartz grains display higher birefringent colors (yellow/orange/brown) in thicker thin sections (50 μm).

Photo 31. Ione sandstone (#92-02), Road outcrop Hwy 124, Ione (PPL with WRL). View shows a Lower Ione sandstone fabric from a weathered road cut exposure. Goethite precipitation (yellow) is associated with the oxidation of O-F cement coatings (a) and O-F concentrations in the fabric of the clay aggregates (b). The arrangement of goethite cement occurring in the clay aggregate fabric appears related to variations in the amount and arrangement of precursor O-F cement (organo-siliceous) in the clay aggregates. Compare patterns of goethite cement at "a and b" with arrangement of O-F cement in clay aggregates in Photo 29, "b and c".

Photo 32. Ione sandstone (#89-13), mottled horizon in the paleosol at Apricum Hill (PPL with WRL). View shows iron oxide precipitation in a quartzose Lower Ione sandstone. Most of the kaolinite matrix is associated with goethite precipitation (yellow). Hematite precipitation (red) is randomly distributed in the kaolinite fabric but sometimes associated with laminae concentrated with heavy minerals. Amphibole grains (A) show little or no effects of dissolution and many do not exhibit oxidation halos. This thin section was impregnated with colorless epoxy.

APPENDIX B

X-ray Diffractograms

Key to symbols used in X-ray diffractograms:

Treatments:

1. Mg cation saturated / ethylene glycol solvated
2. Mg cation saturated / hydrated to 54% relative humidity
3. K cation saturated / heated at 110°C

Mineral Symbols:

C	cristobalite
G	goethite
Gb	gibbsite
H	halloysite
Hem	hematite
I/S	mixed layer illite-smectite
K	kaolinite
K_β	kaolinite (CuKβ radiation)
Ksp	K-feldspar
L	lepidocrocite
M	mica
Q	quartz
S	smectite
V	vermiculite

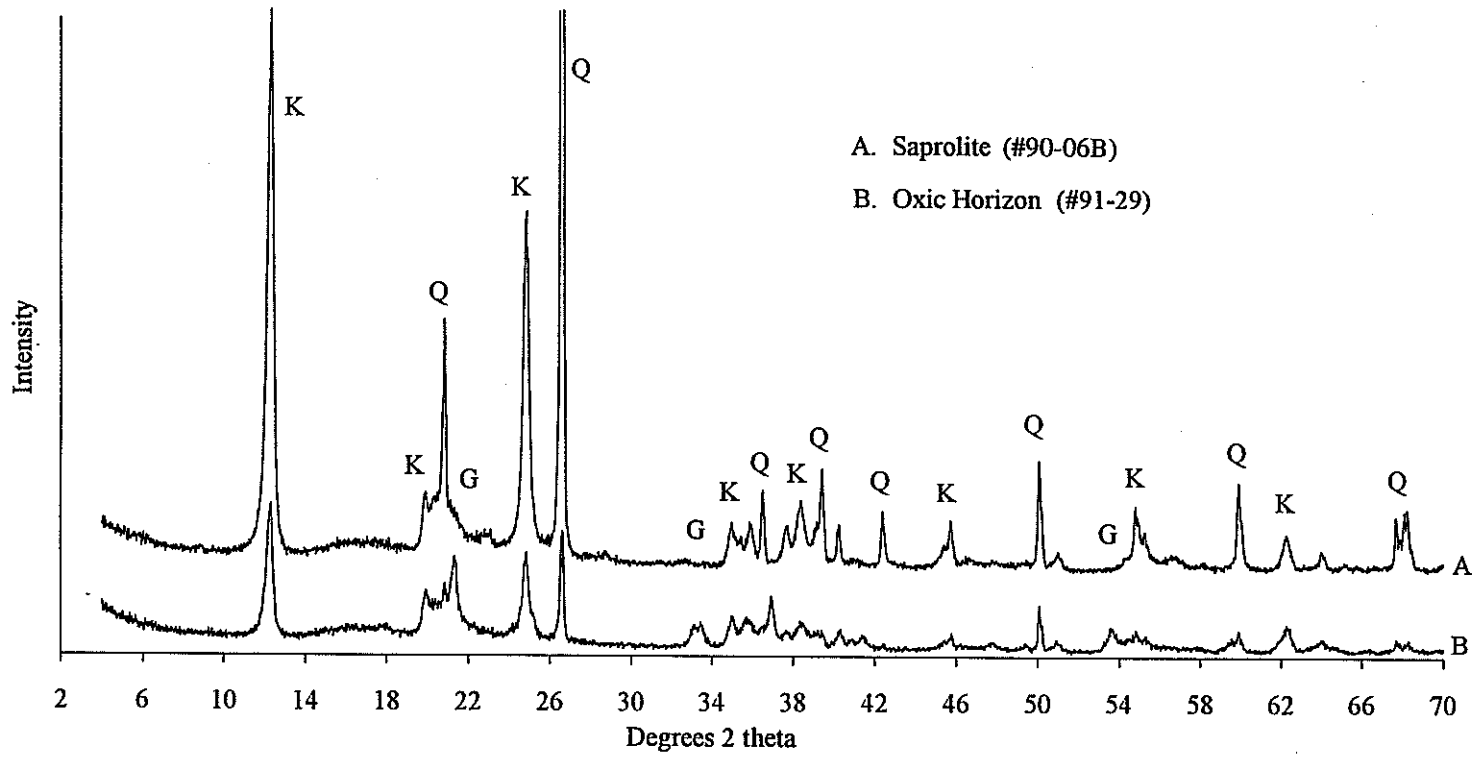

XRD 1. Whole rock analysis of Manzanita Oxisol material.

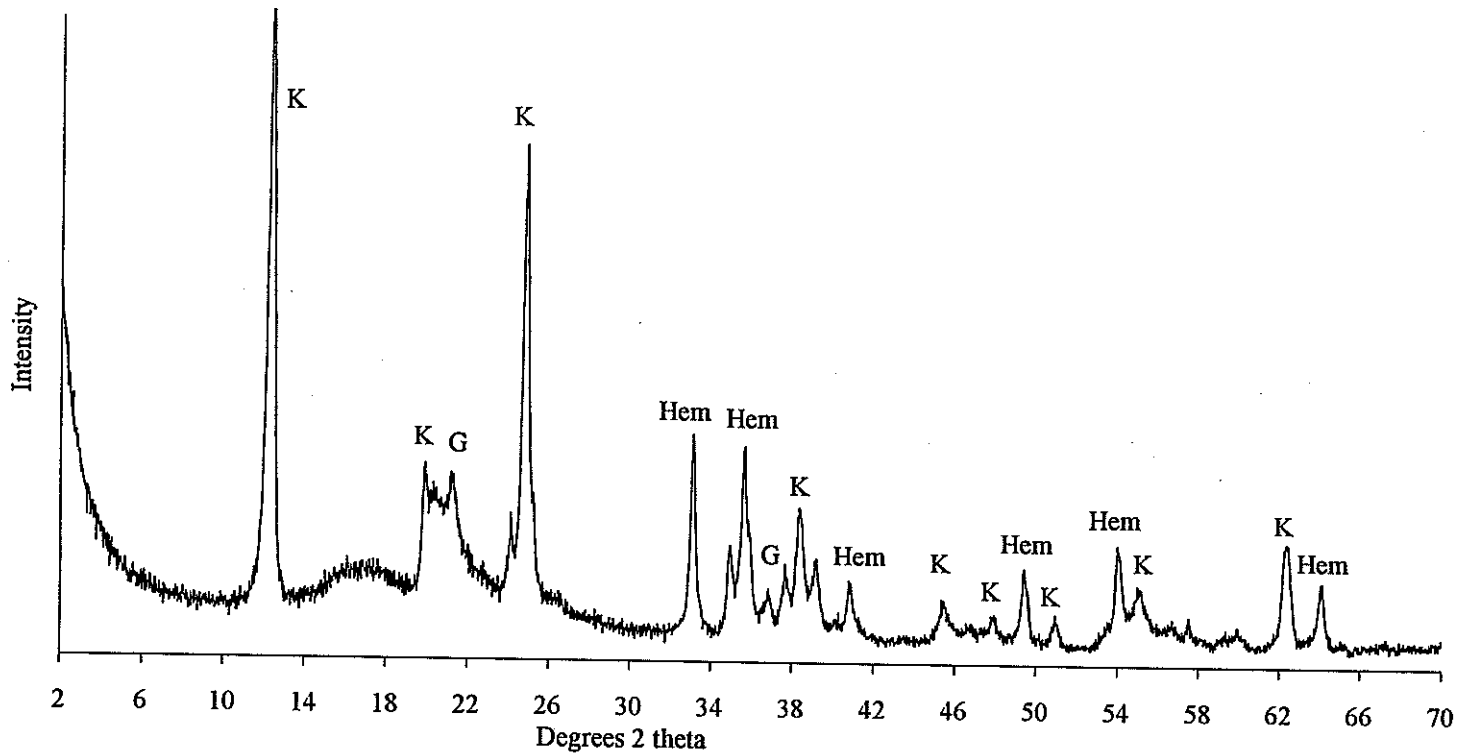

XRD 2. Whole rock analysis of oxic material (#JB-1) from the Jones Butte paleosol, Ione.

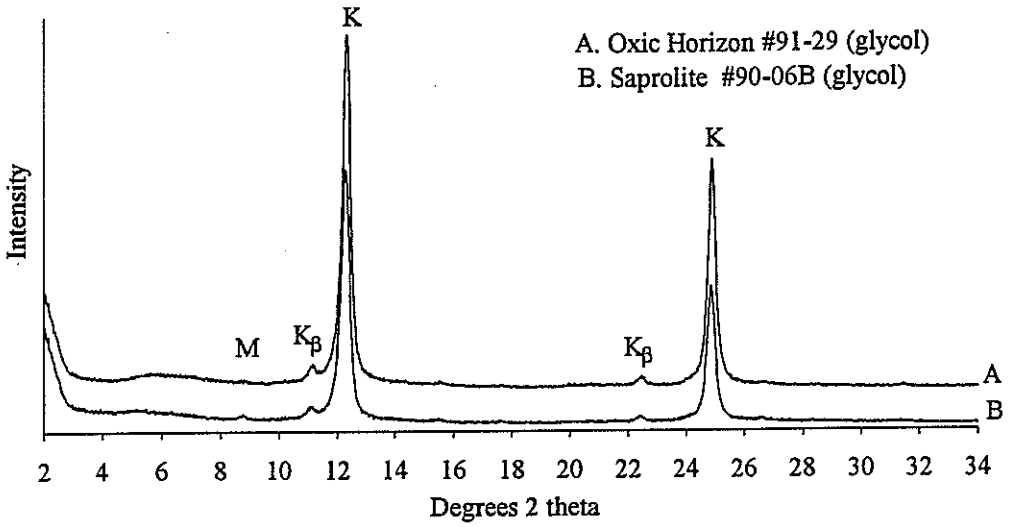

XRD 3. The <2 μm fraction of Manzanita Oxisol material.

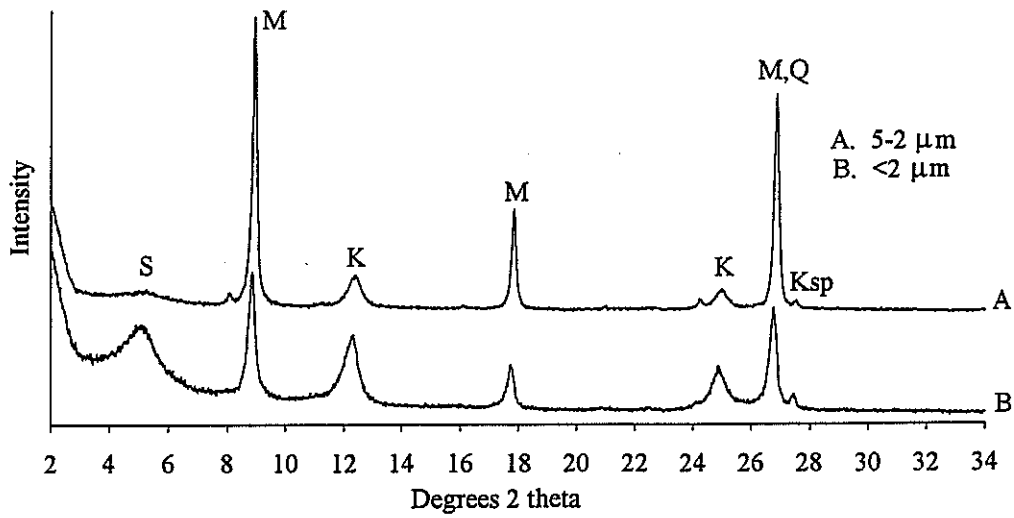

XRD 4. Partially weathered granitic saprolite (#90-10), Manzanita site (glycol).

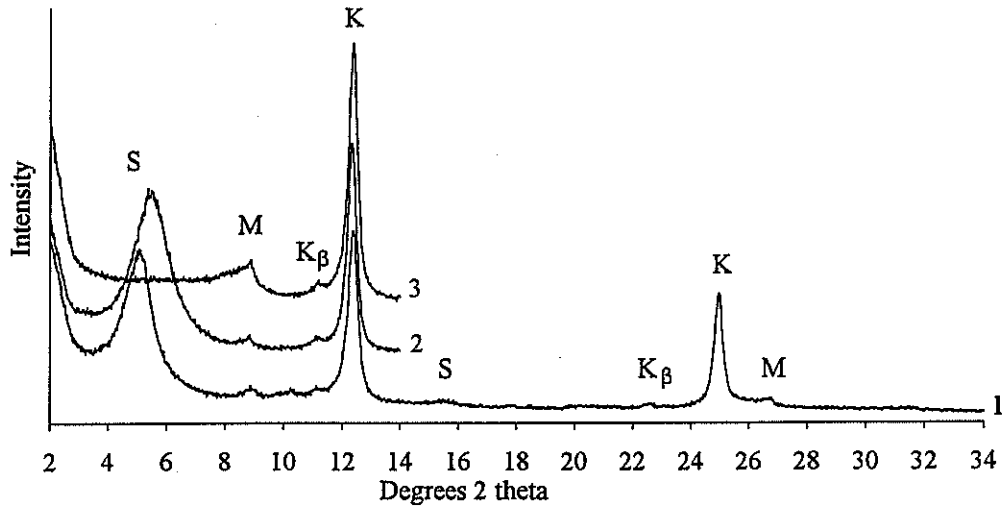

XRD 5. The <2 μm fraction of granitic saprolite (#94-06), Manzanita site.

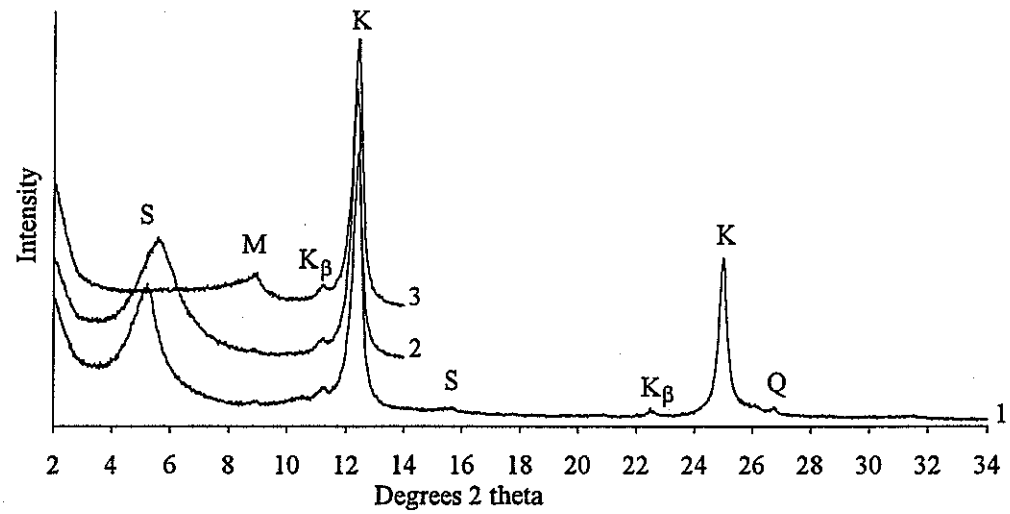

XRD 6. The <2 μm fraction of weathered Ione sediments (#92-30), Manzanita site.

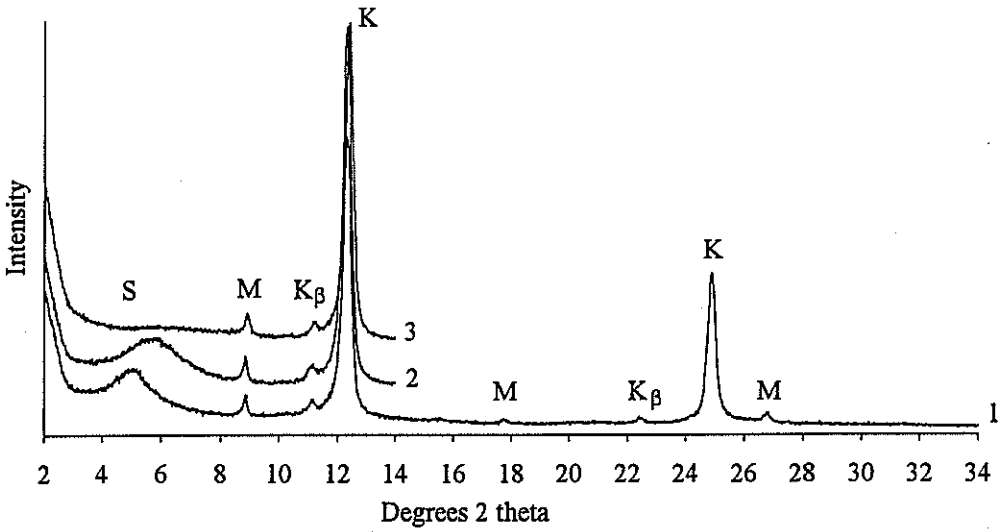

XRD 7. The <2 μm fraction of Lower Ione sandstone (#91-27B), Quaker Hill.

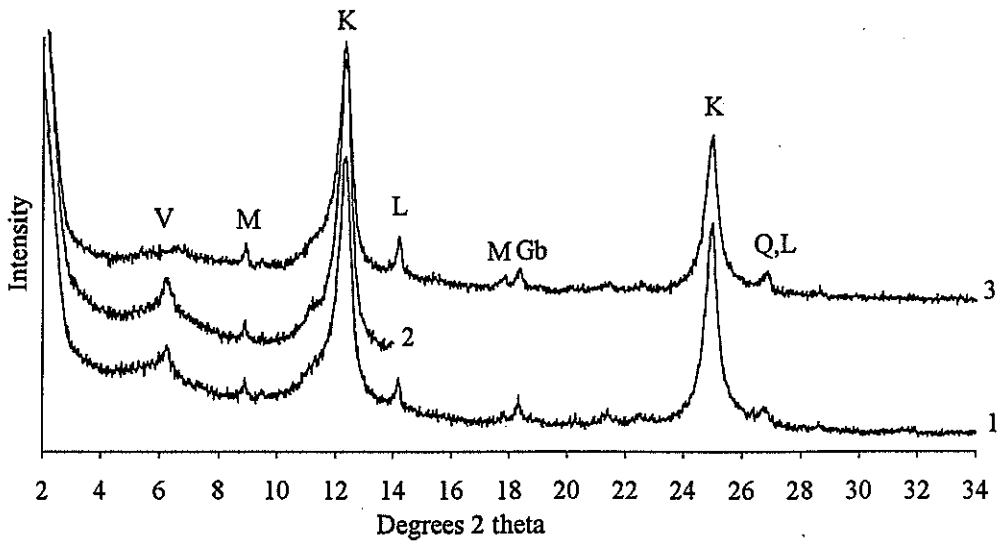

XRD 8. The <2 μm fraction of Lower Ione sandstone (#92-27), Washington.

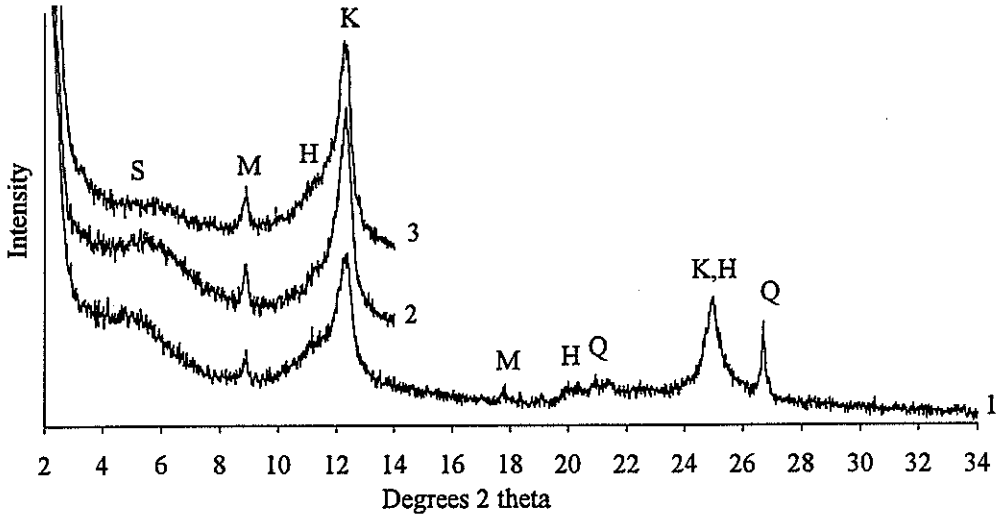

XRD 9. The <2 μm fraction of Lower Ione sandstone (#91-12), Gold Run.

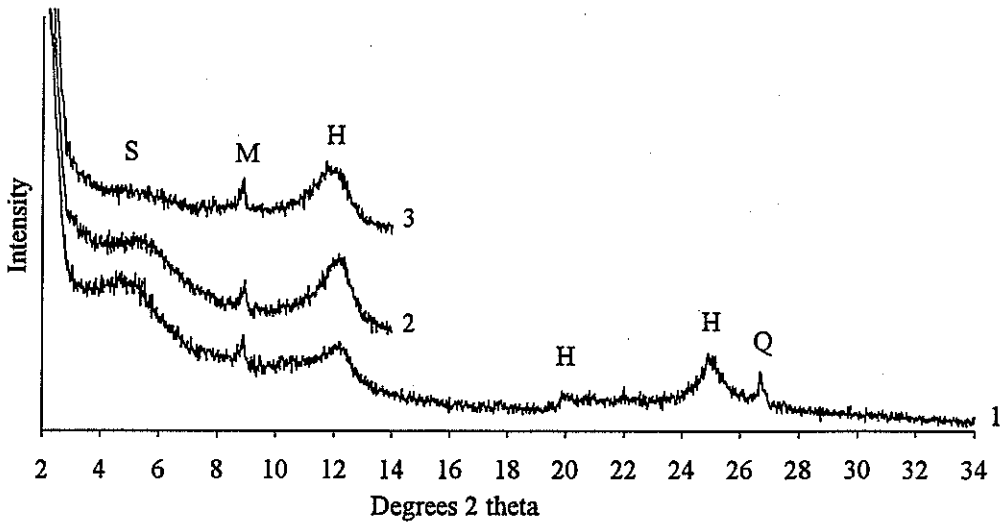

XRD 10. The <2 μm fraction of Ione sandstone (#91-31), Manzanita site.

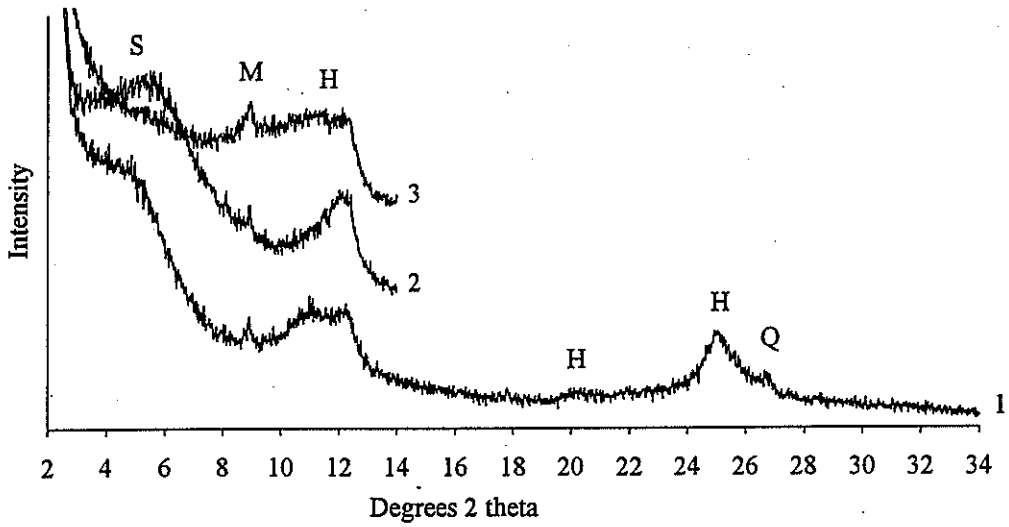

XRD 11. The <2 μm fraction of weathered Ione sandstone (#92-28), Manzanita site.

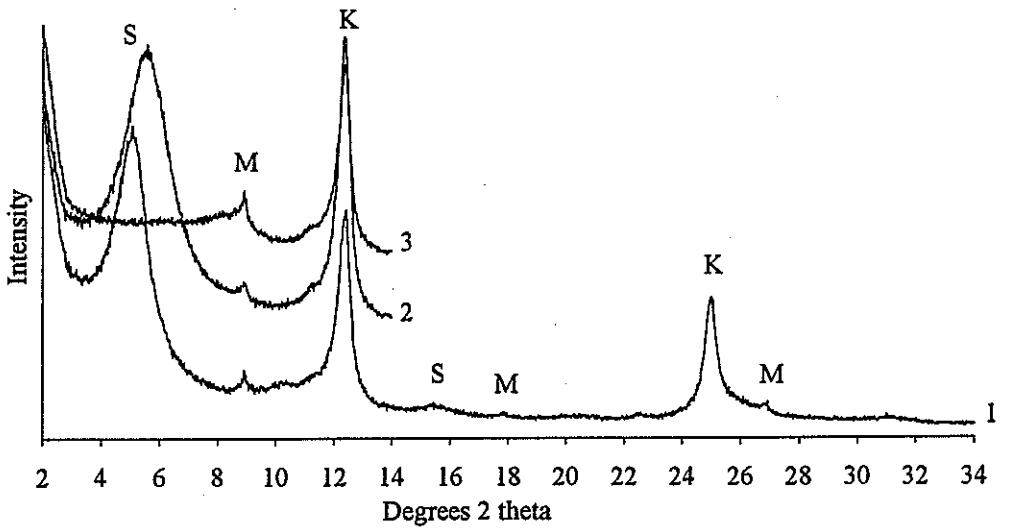

XRD 12. The <2 μm fraction of Upper Ione mudstone (#91-26), Scotts Flat.

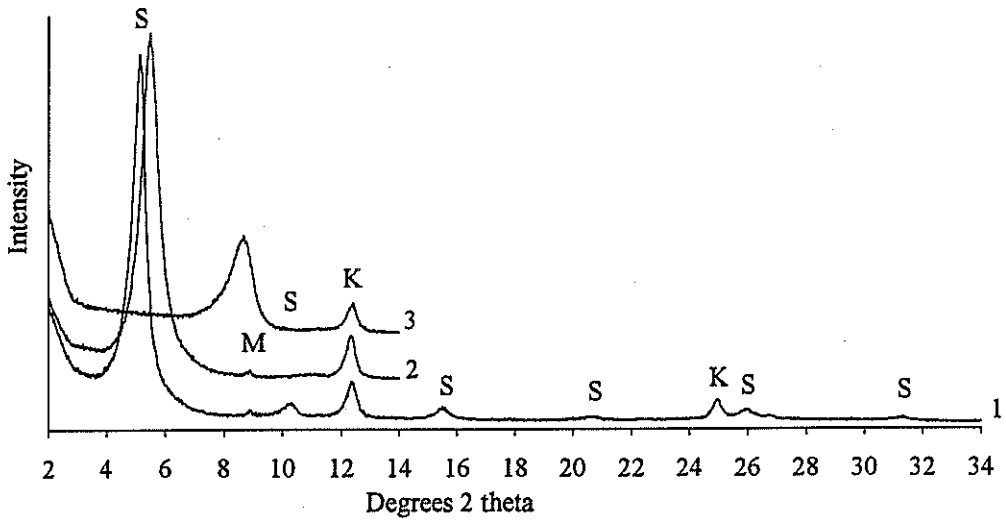

XRD 13. The <2 μm fraction of Upper Ione sandstone (#91-27A), Quaker Hill.

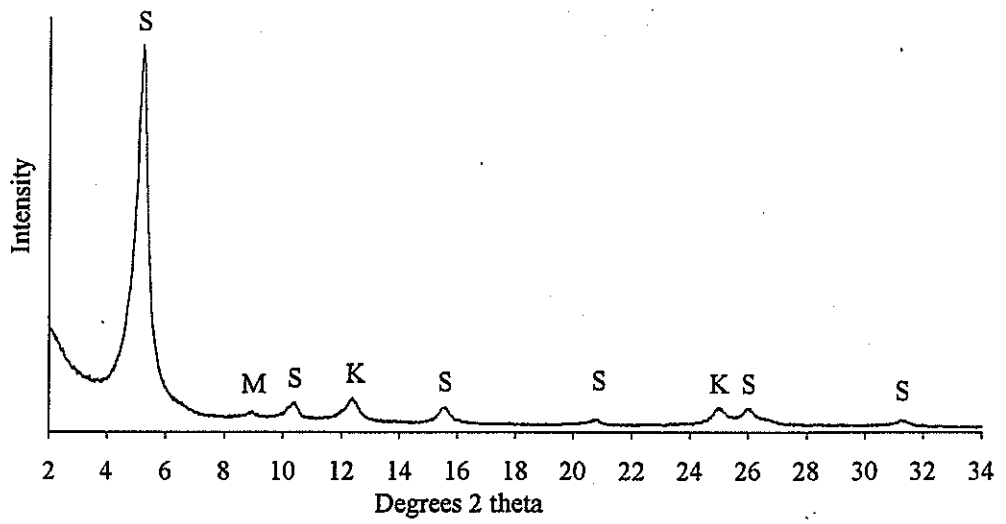

XRD 14. The <2 μm fraction of Upper Ione sandstone (#91-25), Quaker Hill.

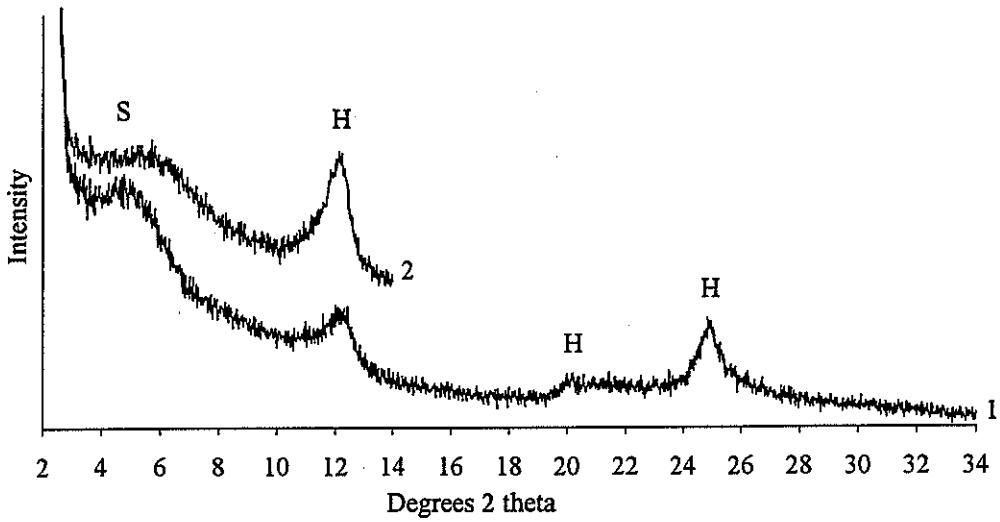

XRD 15. The <2 μm fraction of altered tuff (#91-06), Baxter.

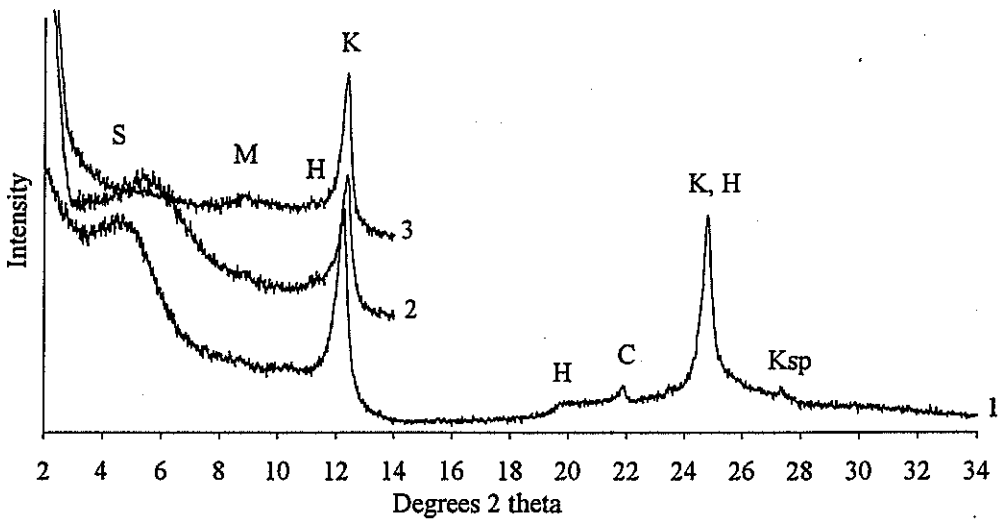

XRD 16. The <2 μm fraction of intervolcanic sandstone (#91-08), Baxter.

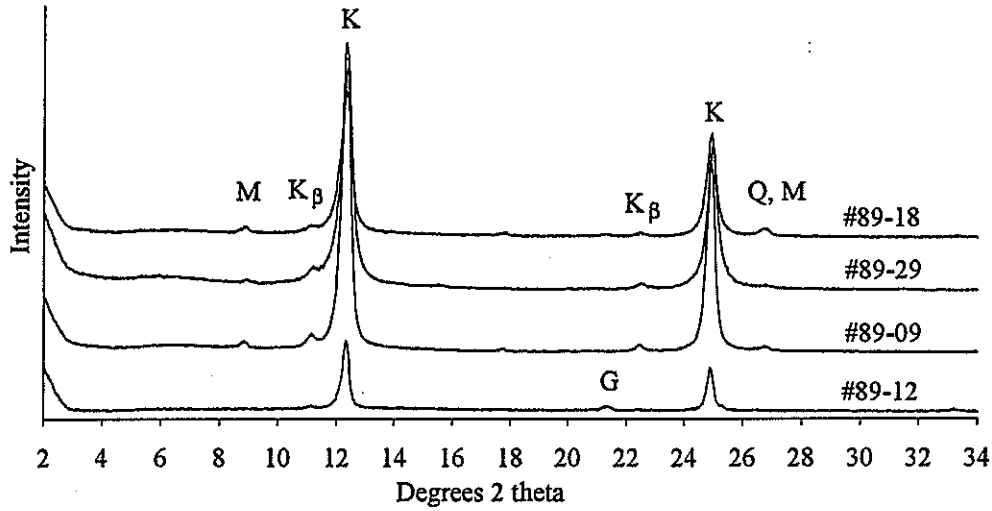

XRD 17. The <2 μm fraction of Lower Ione sandstones, Ione area (glycol patterns).

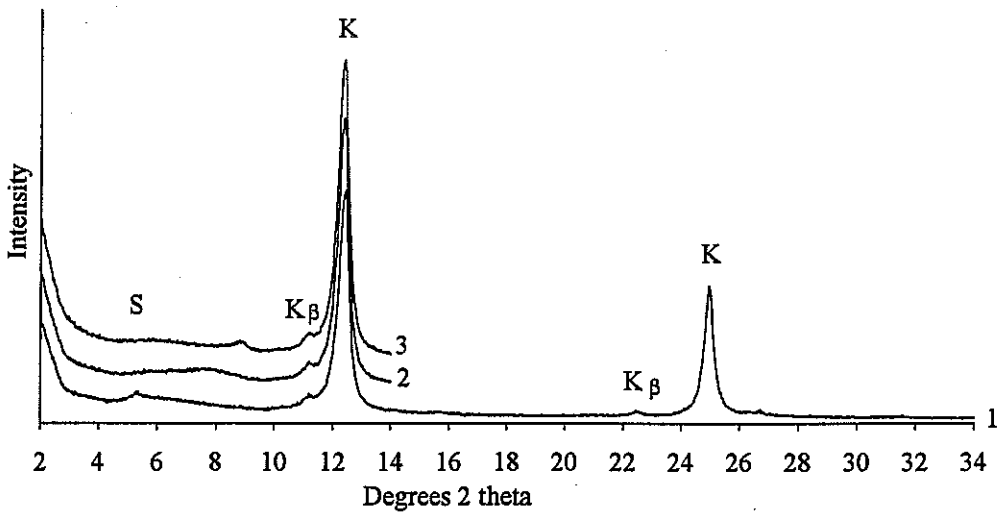

XRD 18. The <2 μm fraction of Lower Ione mudstone (B6), Bacon Pit, Ione.

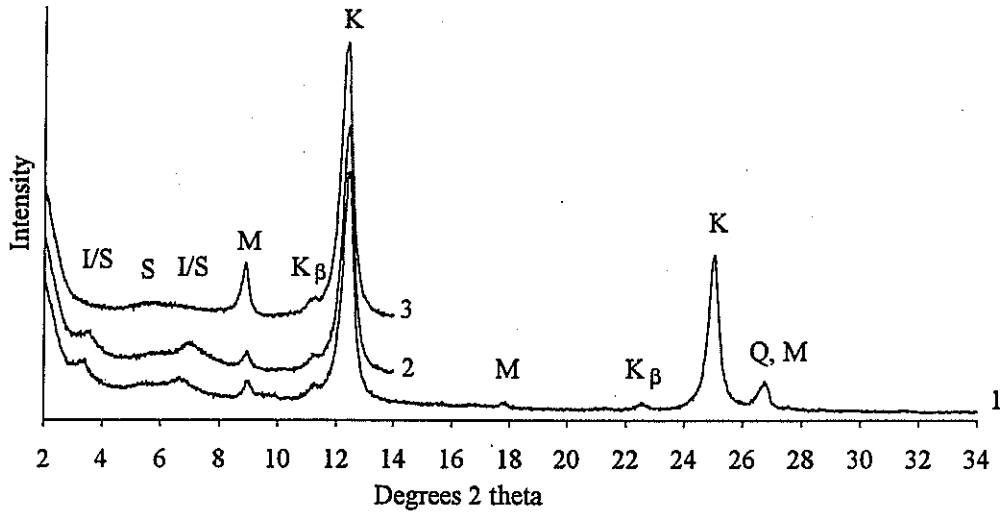

XRD 19. The <2 μm fraction of Lower Ione mudstone (#89-16), Lanes, Ione.

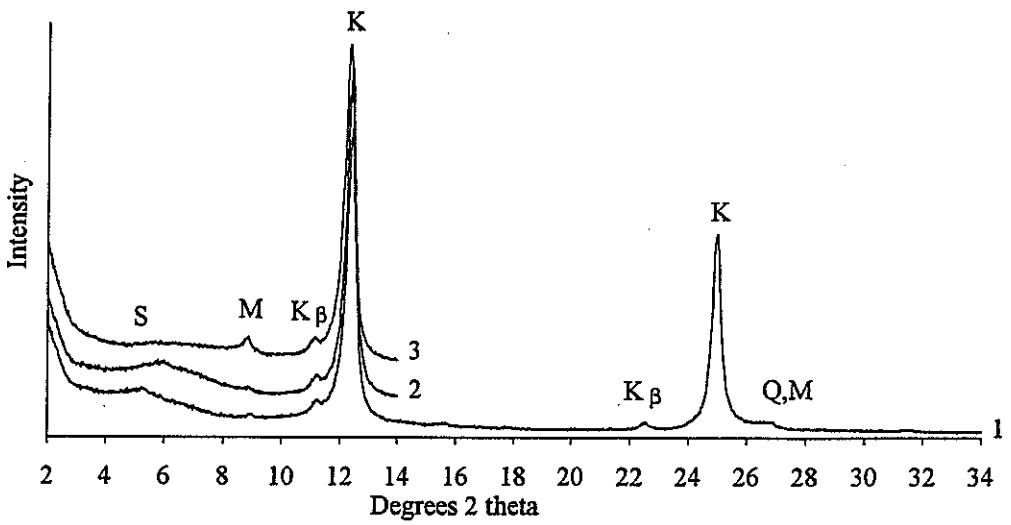

XRD 20. The <2 μm fraction of weathered Ione sandstone (#92-14), Jones Butte, Ione.

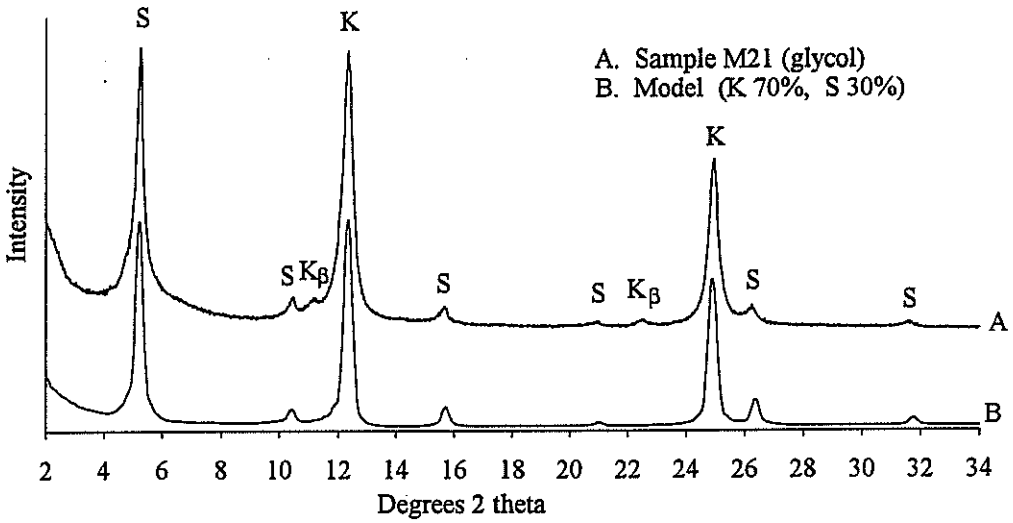

XRD 21. The <2 μm fraction of Lower Ione mudstone (M21), Bacon Pit, Ione.

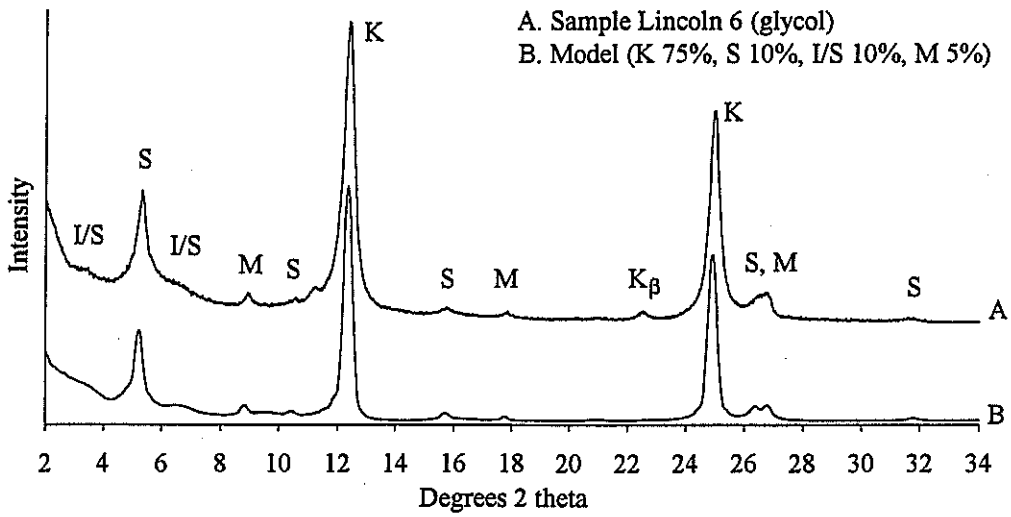

XRD 22. The <2 μm fraction of Lower Ione mudstone (Lincoln 6), Lincoln.

APPENDIX C

EDX Spectra

Key to cation symbols used in EDX spectra:

Al	aluminum
Ba	barium
Ca	calcium
Cl	chlorine
Fe	iron
K	potasium
Mg	magnesium
Na	sodium
S	sulfur
Si	silicon
Ti	titanium

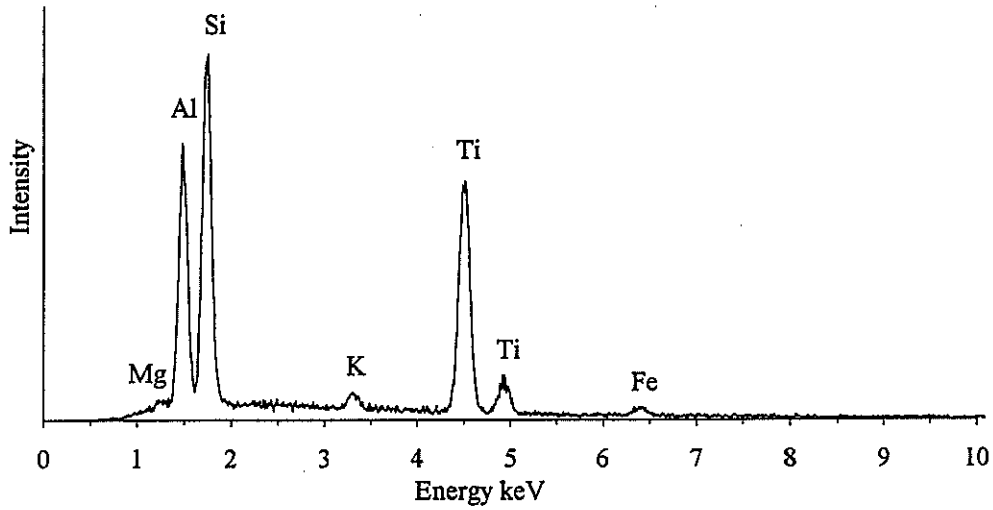

EDX 1. Residual biotite layers in a kaolinized mica grain (#90-07), Manzanita site.

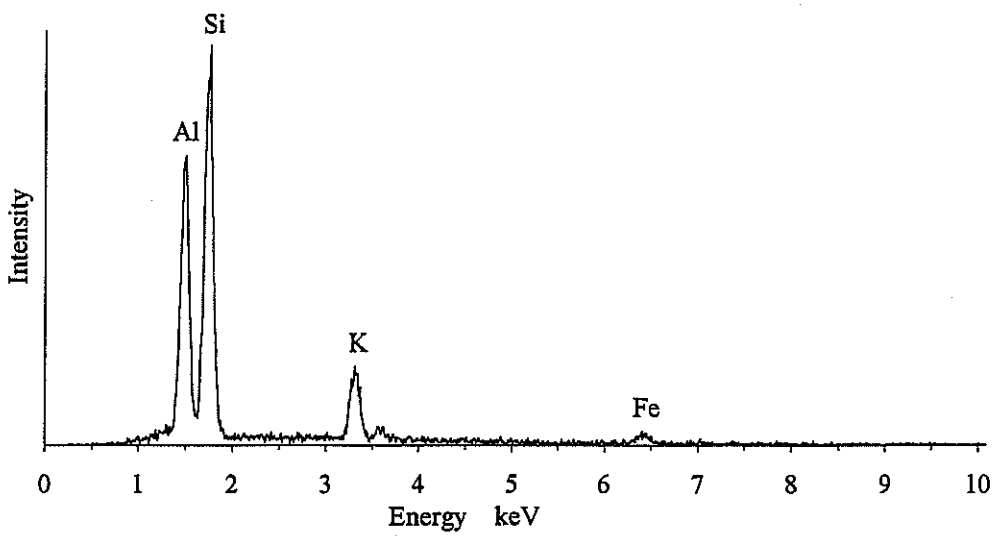

EDX 2. Mica layers in vermicular kaolinite (#90-07), Manzanita site.

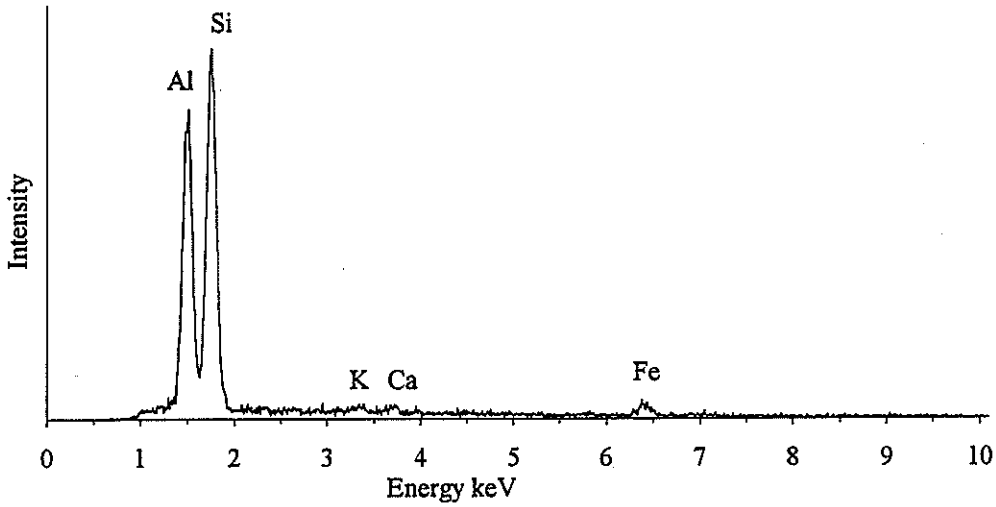

EDX 3. Kaolinite with O-F cement coating (#90-07), Manzanita site.

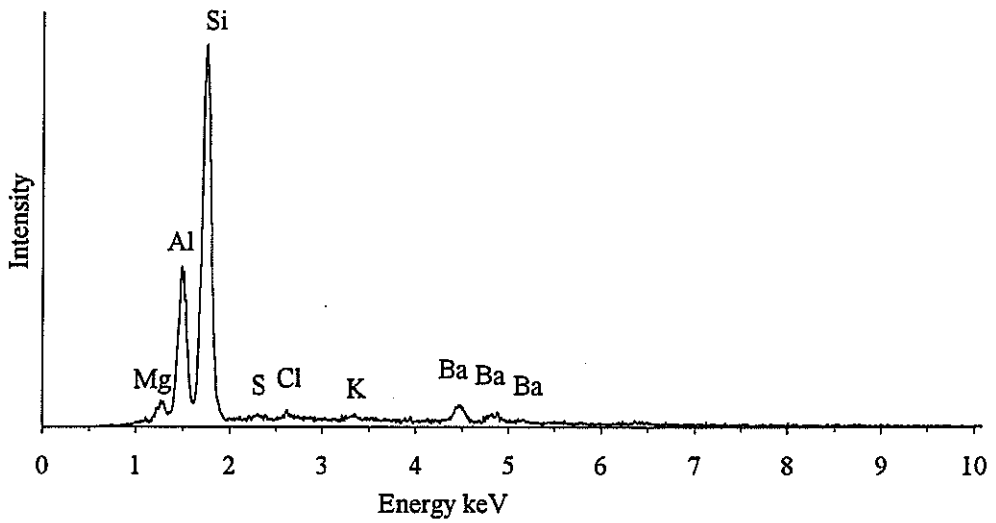

EDX 4. Smectite clay aggregate clast (#91-25), Scotts Flat.

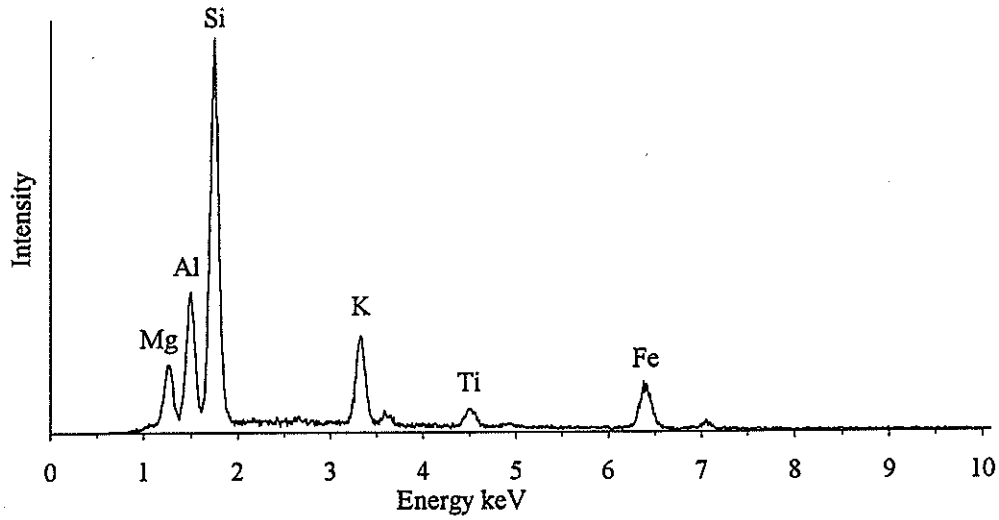

EDX 5. Residual biotite layers in a smectitized mica grain (#91-25), Scotts Flat.

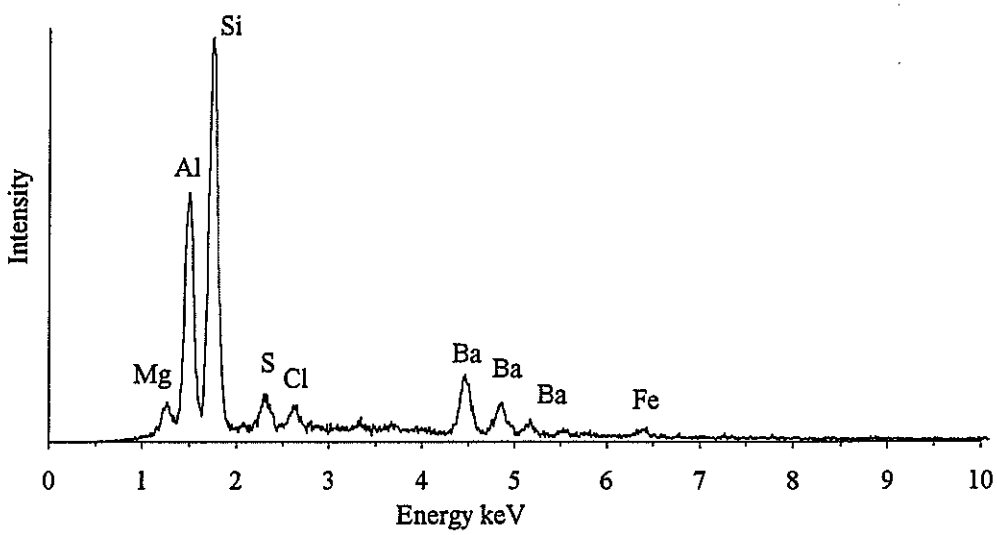

EDX 6. Smectite layers in altered biotite grain (#91-25), Scotts Flat.

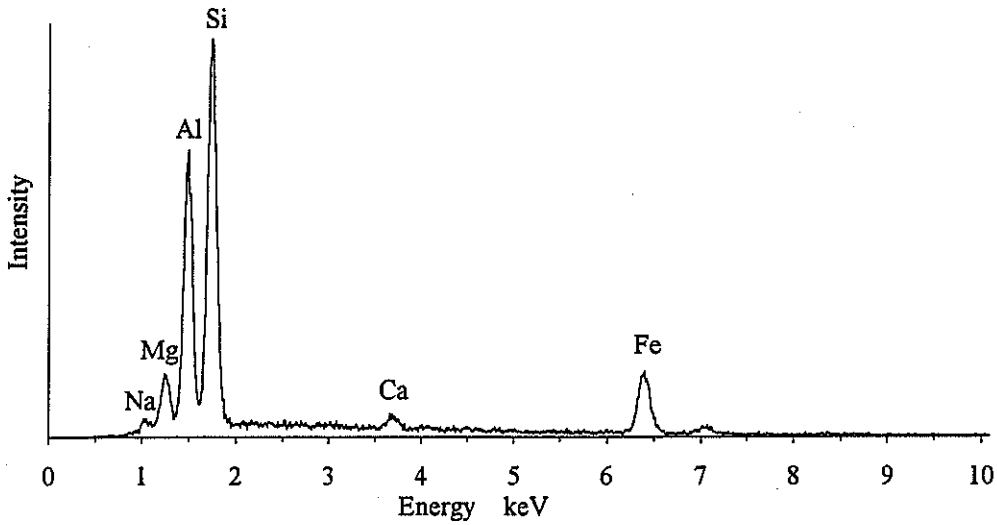

EDX 7. Amphibole grain in Lower Ione sandstone (#89-09), Ione.

Appendix D

Mineral Abundance in Percent in Ione Sandstones

Sample ID	Location	Quartz	Feldspar	Clay Aggregates	Kaolinized Mica	Mica	Rock Fragments	Heavy Minerals	Detrital Mud	Illuvial Clay	Glass Shards	Porosity
Proximal Ione Sandstones												
90-23	Manzanita	33	8	11	0	1	0	1	43	0	0	4
91-31	Manzanita	32	12	22	0	2	1	1	24	0	0	8
92-28	Manzanita	39	16	18	0	2	4	0	2	11	0	10
92-30	Manzanita	57	0	7	0	0	2	0	0	21	0	15
91-12b	Gold Run	45	3	35	4	1	0	1	0	0	0	14
91-27b	Quaker Hill	41	13	28	8	0	1	0	0	0	0	11
92-27	Washington	46	2	44	2	0	0	1	0	0	0	7
91-25	Scotts Flat	35	13	14	0	22	0	0	0	0	0	17
Intervolcanic Sandstone												
91-08	Baxter	8	10	50	0	9	11	0	0	0	4	10
Distal Ione Sandstones												
89-09	Apricum Hill	41	1	42	13	0	0	0	0	0	0	4
89-10	Apricum Hill	33	2	33	30	0	0	0	0	0	0	4
91-16	Owens-Ill Pit	37	1	49	6	2	0	1	4	0	0	2
91-17	Old Sand Plant	45	1	48	3	0	0	2	0	0	0	4
91-19	Wallens Pit	30	1	49	17	0	0	1	0	0	0	4

*Mineral percentages based on 200 points per thin section.

Appendix E

Sample Locations

Sample ID	District	County	Location
B5	Bacon pit, Ione	Amador	Lot 222*
B6	Bacon pit, Ione	Amador	Lot 222*
JB-1	Jones Butte, Ione	Amador	Lot 237*
Lincoln 6	Lincoln	Placer	Gladding McBean Mining Pit
Lincoln 7	Lincoln	Placer	Gladding McBean Mining Pit
M21	Bacon pit, Ione	Amador	Lot 222*
89-09	Apricum Hill, Ione	Amador	sw1/4, nw1/4, sw1/4 of sec 5 T5N R10E
89-10	Apricum Hill, Ione	Amador	sw1/4, nw1/4, sw1/4 of sec 5 T5N R10E
89-11	Apricum Hill, Ione	Amador	sw1/4, nw1/4, sw1/4 of sec 5 T5N R10E
89-12	Apricum Hill, Ione	Amador	sw1/4, nw1/4, sw1/4 of sec 5 T5N R10E
89-13	Apricum Hill, Ione	Amador	sw1/4, nw1/4, sw1/4 of sec 5 T5N R10E
89-14	Apricum Hill, Ione	Amador	sw1/4, nw1/4, sw1/4 of sec 5 T5N R10E
89-16	Lanes, Ione	Amador	se1/4, sw1/4, se1/4 of sec30 T6N R10E
89-18	Lanes, Ione	Amador	se1/4, sw1/4, se1/4 of sec30 T6N R10E
89-26	Jones Butte, Ione	Amador	Lot 237*
89-29	Jones Butte, Ione	Amador	Lot 237*
90-06B	Manzanita pit	Nevada	ne1/4, nw1/4, nw1/4, of sec7 T16N R9E
90-07	Manzanita pit	Nevada	ne1/4, nw1/4, nw1/4, of sec7 T16N R9E
90-10	Manzanita pit	Nevada	ne1/4, nw1/4, nw1/4, of sec7 T16N R9E
90-23	Manzanita pit	Nevada	nw1/4, ne1/4, ne1/4 of sec 12 T16N R8E
91-06	Baxter	Placer	ne1/4, ne1/4 of sec 31 T16N R11E
91-08	Baxter	Placer	ne1/4, ne1/4 of sec 31 T16N R11E
91-12	Gold Run	Placer	ne1/4, se1/4 of sec 4 T15N R10E
91-15	Owens Ill pit, Ione	Amador	Lot 260*
91-16	Owens Ill pit, Ione	Amador	Lot 259*
91-17	Old sand plant, Ione	Amador	Lot 271*
91-18	Old sand plant, Ione	Amador	Lot 271*
91-19	Wallens pit, Ione	Amador	Lot 265*
91-25	Scotts Flat	Nevada	sw1/4, ne1/4, ne1/4 of sec 12 T16N R9E
91-26	Scotts Flat	Nevada	sw1/4, ne1/4, ne1/4 of sec 12 T16N R9E
91-27A	Quaker Hill	Nevada	ne1/4, sw1/4, ne1/4 of sec7 T16N R10E
91-27B	Quaker Hill	Nevada	sw1/4, nw1/4, se1/4 of sec7 T16N R10E
91-28	Manzanita	Nevada	nw1/4, ne1/4, ne1/4 of sec 12 T16N R8E
91-29	Manzanita	Nevada	nw1/4, ne1/4, ne1/4 of sec 12 T16N R8E
91-31	Manzanita	Nevada	nw1/4, ne1/4, ne1/4 of sec 12 T16N R8E
92-01	Hwy 124, Ione	Amador	Lot 261*

92-02	Hwy 124, Ione	Amador	Lot 261*
92-12	Jones Butte, Ione	Amador	Lot 237*
92-14	Jones Butte, Ione	Amador	Lot 237*
92-27	Washington	Nevada	swl/4, nel/4, nwl/4 of sec 13 T17N R10E
92-28	Manzanita	Nevada	nwl/4, nel/4, nel/4 of sec 12 T16N R8E
92-29	Manzanita	Nevada	nwl/4, nel/4, nel/4 of sec 12 T16N R8E
92-30	Manzanita	Nevada	nwl/4, nel/4, nel/4 of sec 12 T16N R8E
94-05a	Manzanita	Nevada	nwl/4, nel/4, nel/4 of sec 12 T16N R8E
94-06	Manzanita	Nevada	nwl/4, nel/4, nel/4 of sec 12 T16N R8E

All range and township locations are referenced to the Mt. Diablo principal meridian and baseline.

*Lot numbers refer to Arroyo Seco Ranch subdivisions.